MUK PUBLICATIONS
Open Access Publisher

Medical Interface for Echographic Free-hand Images

J. B. Santos[1], D. Celorico[1], J. Varandas[2] and J. Dias[2]

[1]*Department of Electrical Engineering and Computers, Institute of Science and Materials Engineering*
University of Coimbra, polo II, 3030-290 Coimbra, Portugal

[2]*Department of Electrical Engineering and Computers, Institute of Systems and Robotics*
University of Coimbra, polo II, 3030-290 Coimbra, Portugal

This paper deals with the development of a medical imaging interface which primary goal is the 3D reconstruction of human organs from 2D ultrasound images. This particular tool was developed to work with a conventional ultrasound probe having a position sensor attached to it. Important requirements like acquisition, calibration, segmentation, interpolation and visualisation for 3D reconstruction are provided by this friendly interface. This tool was developed in C++ language integrating some Matlab executable files and the Visualization Toolkit (VTK) that is free software oriented for 3D graphical computation, visualization and image processing. In this work, we concentrated our efforts in the procedures for the volumetric reconstruction of the Left Ventricle (LV). Special attention is dedicated to the segmentation of the LV contours due to its importance to the 3D volumetric reconstruction. This is not an easy task when the 2D images are noisy and the LV boundaries are not clear as is the case verified this work.

Keywords: Medical images, volumetric images, ultrasound

1. INTRODUCTION

Echocardiography is a valuable non-invasive tool for imaging the heart and surrounding intrathoracic structures and is an essential way to diagnosis heart diseases. Concerning to the LV, the endocardial and epicardial boundaries are useful quantitative measures for various cardiac functions such as pressure-volume ratio, ejection fraction and cardiac wall motion. In order to quantify these measures the contour of the LV should be extracted. The extraction of the LV boundaries by image processing techniques is a hard task inherent to the quality of the 2D images, namely due to their low spatial resolution, high level of speckle noise, and to the poor definition of the myocardial boundaries. Of course that some of these problems are more or less pronounced according to the quality of the used equipment.

Manual tracing of these borders requires an expert and besides, it is a time consuming and a labour intensive task, when a large number of images need to be analysed.

Automatic boundary extraction from echocardiographic images thus, appears as a clinical important need to produce most effective and reliable results. In spite of many researchers have attempted to identify the LV boundaries on 2-DE images, automatically or semi-automatically [Melton 1983, Chu 1988, Detmer, 1990, Setarehdan & Soraghan 1998, Frangi, A. & al. 2001, Xujiong, Y & Noble, J. A. 2002], this goal still is a challenge.

The LV contour extraction is based on the radial search-based approach, where the intensity profiles along a set of equiangular radial lines emanating from the centre point of the LV are analysed. To improve the robustness of the detection, an additional and complementary approach making use of parallel lines traced along with the small dimension of the LV will also be implemented.

The volumetric reconstruction is based on filling an isotropic structure of voxels. Since a point can be located between voxels or a voxel can have more than one or none points, interpolation techniques are required. This tool allows the user to select three distinct interpolation processes: closest neighbour interpolation, Gaussian Splatter method and Shepard method (inverse method of weighed distance). The last section of this paper deals with the application of 3D images visualisations techniques. The user has three options: ray casting, isosurfaces and slicing.

2. B-SCAN IMAGE ACQUISITION

The 2D echographic images were acquired from an ultrasonic equipment from SonoSite (model: SonoSite Titan) with a conventional probe and a position sensor attached to it. This sensor works as a receiver of an electromagnetic position sensor (MiniBIRD_Model 500). The images are visualised in real time, allowing the user to select them at the same time as he performs the scanning. Figure 1 illustrates the front page of the application and figure 2 shows the acquisition process showing a 2D image of the heart called apical long-axis four-chamber view.
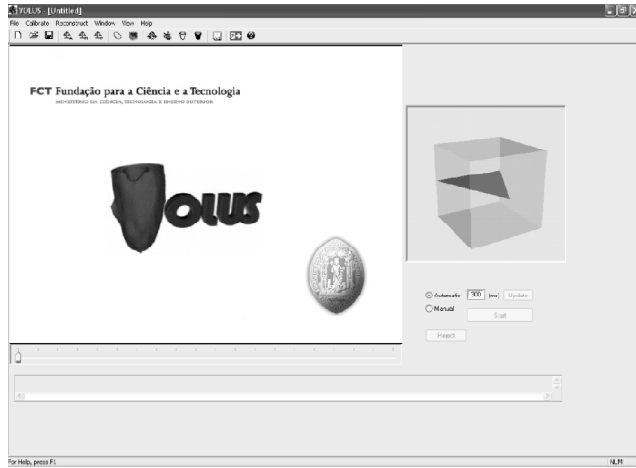
Figure 1: First Page of the User Interface

When the user selects an image (B-scan) its position and orientation is registered using the position sensor. This information is registered for all acquired images and is used to determine the positions and orientations of the B-scans with respect to the fixed transmitter. The following procedure consists of the calibration of the system. This is an important requirement for the freehand images collection.
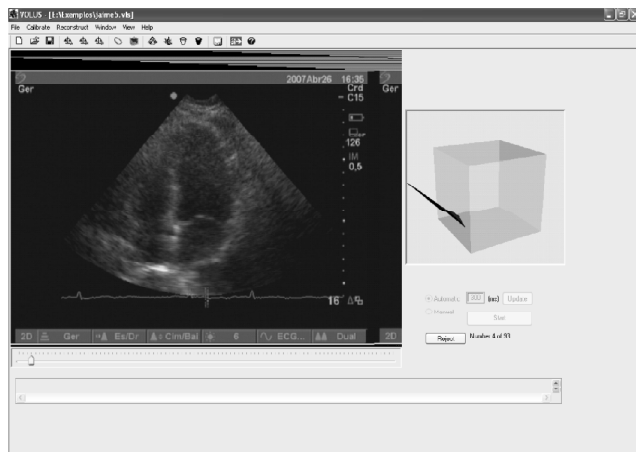
Figure 2: A 2D Image of the Heart: Apical Long-axis Four-Chamber View

3. CALIBRATION PROCEDURE

Calibration implies the calculation of the position and orientation of the 2D images relating to the sensor attached to the probe. The results of calibration (six parameters: three for position and three for orientation) are used to calculate the correct position of each image pixel in a three-dimensional space, allowing the volume reconstruction in an accurate way. This tool allows the calibration process being accomplished in two different ways: manual and automatic. In general, the calibration problem can be formulated by the following equation [Varandas 2004]:

$$m = {}^{M}T_{O} \cdot {}^{O}T_{P} \cdot {}^{P}T_{I} \cdot q \qquad (1)$$

with

$$q = \begin{bmatrix} s_x \cdot u \\ s_y \cdot v \\ 0 \\ 1 \end{bmatrix}$$

where the matrix ${}^{P}T_{I}$ denotes the transformation from B-scan image coordinates frame {I} to the position sensor on the ultrasound probe with coordinates frame {P}. The transformation ${}^{O}T_{P}$ describes the relation between the position of the receiving sensor and the coordinates of the transmitter. The transformation ${}^{M}T_{O}$ represents the relation from the transmitter coordinates to the coordinate frame on the scanned volume. The variables u and v are the column and row indices of the pixel in the B-scan image, and s_x and s_y are the corresponding scaling factors (mm/pixel).

The coordinates of each a pixel are expressed in the coordinate system of the position sensor P (see Fig. 3) but they must be registered in the reconstruction volume with a referential frame {M}. The matrix T illustrated in eq. (1) represents the rigid body transformation from a generic coordinate system {J} to generic coordinate system {K}:

$$^{K}T_{J}(x, y, z, \alpha, \beta, \gamma) \qquad (2)$$

$$= \begin{bmatrix} c\alpha c\beta & c\alpha s\beta s\gamma - s\alpha c\gamma & c\alpha s\beta c\gamma + s\alpha s\gamma & x \\ s\alpha c\beta & s\alpha s\beta s\gamma + c\alpha c\gamma & s\alpha s\beta c\gamma - c\alpha s\gamma & y \\ -s\beta & c\alpha s\beta s\gamma & c\alpha s\beta c\gamma & z \\ 0 & 0 & 0 & 1 \end{bmatrix}$$

where $c = \cos$ and $s = \sin$ were used for simplicity sake, the six degrees of freedom (a, b, g) characterise the rotation and (x, y, z) the translation. The rotation between two coordinate systems is carried out by first rotating through γ around the x-axis, then through β around the y-axis, and finally through α around the z-axis.
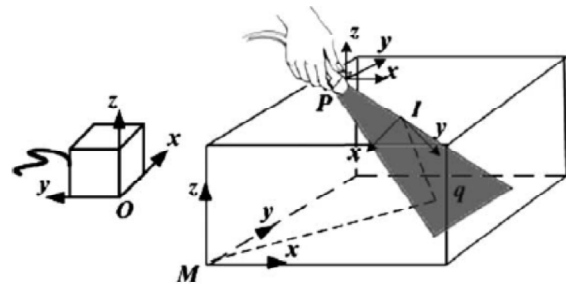
Figure 3: Coordinate Systems of the Reconstruction and Calibration Process: Image Referential (I), Position Sensor Referential (P), Transmitter Referential (O), Volume Referential (M)

The calibration consists of the estimation of matrix ^PT_I, matrix ^MT_O, and the coefficients s_x and s_y, according to Equation 1. From the 14 unknown parameters only eleven will be identified for which, there are many possible methods. The used device for calibration is similar to the Cambridge phantom [Varandas 2004]. The technique is based on the scanning of the bottom of a container with water where each acquired B-scan image has one line that represents the intersection of the ultrasound beam with the bottom of the container. Assuming the bottom of the container is planar, all these lines are in the same plane and the coordinate system {M} is defined at the level of the bottom of the container, with the z-axis exactly orthogonal to this, and then the pixels of the line have to satisfy the following equation:

$$\begin{bmatrix} x \\ y \\ 0 \\ 1 \end{bmatrix} = {}^MT_O \cdot {}^OT_P \cdot {}^PT_I \cdot \begin{bmatrix} s_x \cdot u \\ s_y \cdot v \\ 0 \\ 1 \end{bmatrix} \quad (3)$$

In Eq. (4) the zero component can be written as a function of unknown parameters f and measured the parameters q as:

$$0 = f(\theta, \phi). \quad (4)$$

For each a line in the image it is possible to select two pixels. That defines a line, thus providing two equations for each a B-scan.

An initial estimative can be obtained using a classic optimisation algorithm such as the Levenberg-Marquardt algorithm [More 1977] using for this purpose a minimum of 11 non-linear equations.

The automatic procedure uses all acquired images in the parameters calculation, which could lead to a calibration less effective when the images present poor quality. On the other hand, the manual calibration gives best parameter values, since all bad images can be rejected. However, it is a time consuming process when compared with the automatic one.

4. IMAGES SEGMENTATION

For volumetric reconstruction of the ventricle cavity it is first necessary to extract its boundaries. In this work, we apply a method that is a combination of radial and parallel search-based edge detection. Before proceeding with its application, some image pre-processing is necessary to reduce the noise and enhance the edges of the ventricular boundary. Also the creation of a region of interest (ROI) will reduce the processing time. The ROI characterisation is made after a preview location of the cavity centre point. The results provided in this work were based on a manual centre point extraction. Considering that a reasonable number of images for volumetric reconstruction is about

25, this task is not too time consuming and, as an advantage, allows a much more precise reconstruction compared to an automatic selection of the centre point. After the location of the centre point, the image is divided in two sections (left and right) both referenced to an axis passing by the central point as illustrated in Figure 4. These two sections are then divided in small rectangular blocks. For each block a threshold is obtained using the Otsu's method [Otsu 1979]. Formulated as discriminant analysis, the method separates pixels into two classes (objects and background), by a threshold. The criterion function involves between-classes variance (σ_b^2) to the total variance (σ_t^2), and is defined as:

$$\eta = \frac{\sigma_b^2}{\sigma_t^2} \quad (5)$$

All possible thresholds, through each selected block are evaluated in this way, and the intensity that maximizes this function is the optimal threshold.
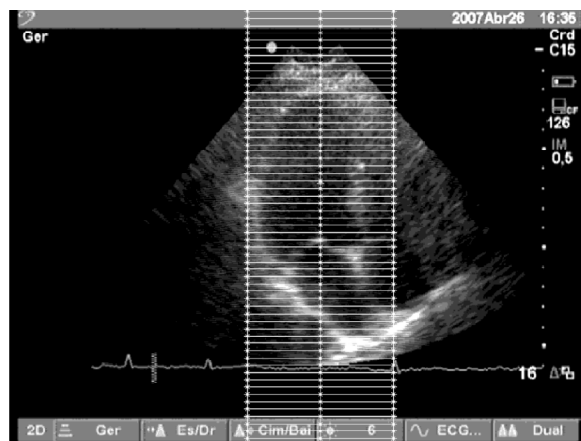
Figure 4: ROI Selection

At the end of this operation the LV boundaries were clearly more pronounced, however, the contours were not totally closed and additionally the cavities presented some noise. Some improvement was achieved by using morphological operations such as dilation and erosion. The dilation operation adds pixels to the boundaries of objects in an image, while erosion removes pixels from object boundaries. The number of pixels added or removed depends on the size and shape of the structuring element used to process the image. Based on this morphological operations it was performed the image closure followed by image opening with a square as a structuring element, thus, allowing that the location of the boundaries remain approximately in the same locations (see Fig. 5).

As illustrated in Figure 5, it is obvious that the extraction of boundaries could still be erroneous due to some remaining noise observed into the cavity. To guaranty an unambiguous identification of LV boundaries

by the combined method of radial and parallel search-based edge detection, an additional step was introduced in the algorithm.
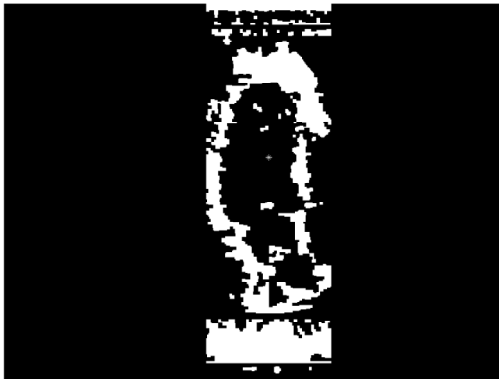
Figure 5: ROI After Morphological Operations: Erosion and Dilation

This step consisted of splitting the cavity in four quadrants and performing edge detection through each quadrant line. This process, associated with the application of a function of boundary tracing, permitted to evaluate the LV contour though neither totally closed nor smoothed. This goal was reached by a combination of the radial and parallel edge detection approaching mentioned. In the radial approach it was used an ellipse, centred at the centre point of the ventricle, and the intensity profiles were extracted along its radials. This results in a high density of points in the upper and lower region of the ventricular cavity and much less points in the left and right sides. To reduce the uncertainty in the LV walls detection a parallel approach was used, like the one shown in Figure 4. Here the intensity profiles were extracted along the parallel lines from the central axis to the right and left sides.

The next step consisted of the elimination of all points outside the cavity region, based on restriction conditions. Then we proceeded with the smoothing of the extracted LV edge points followed by the application of a cubic spline interpolation, as illustrated in Figure 6.
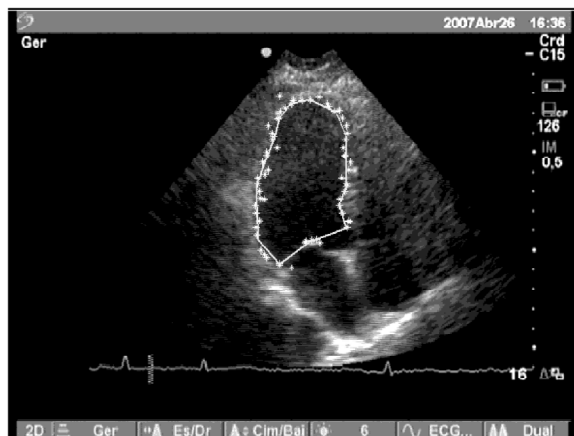
Figure 6: Extracted Boundary Points and Contour Tracing

It is important to mention that the processed images were very noisy. Most of them presented ill-defined boundaries making the reconstruction process very laborious, as was demonstrated before. Of course that with images like the one shown in Figure 7, obtained from a higher resolution echographic machine, procedures are easier, essentially due to the fact that LV boundaries present a very good contrast when compared with the cavity region.
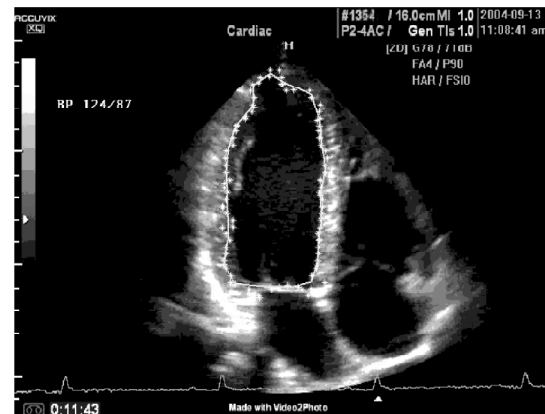
Figure 7: Application of the Technique to Higher Quality Images

The LV tracing points resulting from the segmentation procedure, for each image, can be used by the application to create a mask. In the reconstruction path, the masks are very useful to produce a model of the left ventricular cavity.

5. INTERPOLATION

The volume reconstruction is based on filling an isotropic structure of voxels (volume unit) with each voxel having an associated luminance level. To determine this level it is necessary to identify the regions of interest in the two-dimensional images (B-scans) and localize them into the space. With the use of the information regarding to the coordinate position and orientation of each pixel in the image it is possible to determine its position in the 3D space. However a point can be located between voxels or a voxel can have more than one or none points, so it becomes necessary to use interpolation techniques. These techniques rely on processes of constructing new data points with a specific attribute from a discrete set of known data points in the same area or region.

The developed application allows the user to select three distinct interpolation processes: closest neighbour interpolation, Gaussian Splatter method and Shepard method (inverse method of weighed distance). The interpolation method of the closest neighbour (implemented using vtkSurfaceReconstructionFilter) is based on the volume construction by identification of surfaces inside it [Hoppe 1994]. This interpolation surface corresponds to places were a function (that depends on

the distance of points to the limit of the object) is equal to a constant (f (x, y, z) = c).

The Gaussian Splatter method (implemented using vtkGaussianSplatter) is based on the Gaussian distribution function. This interpolation technique uses the point data in a voxel structure and interpolates these point attribute values with the voxels according to the Gaussian distribution. The uniform Gaussian distribution centred at a point p_i can be cast in the form [Shroeder & al 2004]:

$$G(x, y, z) = se^{-f\left(r/R\right)^2} \tag{6}$$

where s = a scale factor; f exponent scale factor; $r = \|p-p_i\|$ is the distance between any point and the Gaussian centre point; and R is the radius of influence of the Gaussian.

The Shepard method (implemented using vtkShepardMethod) is a weighted inverse distance interpolation technique, which attributes a weight to each point. For each voxel, it is calculated the distance to every point and the weight attributed is dependent on that distance, thus, points that are closer have more weight decreasing then exponentially with the increased distance. Mathematically, given a set of points $p_i = (x_i, y_i, z_i)$ and the function values $F_i(p_i)$, the new points can be interpolated using the equation [Shroeder & al 2004]:

$$F(p) = \frac{\sum_{i=1}^{n} \dfrac{F_i}{\left|p - p_i\right|^2}}{\sum_{i=1}^{n} \dfrac{1}{\left|p - p_i\right|^2}} \tag{7}$$

6. VISUALISATION

The visualisation of 3D images can be made by volume rendering, slicing or surface rendering. This tool allows the technician to visualise the voxels structure by implementing one of the following three options: ray casting, isosurfaces and slicing.

6.1. Volume Rendering

In order to visualize a volume, the ray casting method which is based on the Blinn/Kajiya model [Watt & Watt 1992] is a technique widely used. It permits visualizing sampled functions of three spatial dimensions by computing 2D projections of a colored semitransparent volume. It basically consists in casting a ray from a given position with a given direction, tracing rays from the view point into the viewing volume. In this model we have a volume which has a density D(x, y, z), penetrated by a ray R. At each point along the ray there is an illumination I(x, y, z) that comes from the light source and reaches the point (x, y, z). The intensity scattered along the ray depends on the intensity value on a reflection function or phase function P and on the local density D(x, y, z). Along the ray the density function and the illumination from the source are parameterized as:

$$D(x(t), y(t), z(t)) = D(t) \tag{8}$$

$$I(x(t), y(t), z(t)) = I(t) \tag{9}$$

The illumination scattered along R from a point distance t along the ray is given by:

$$I(t)\, D(t)\, P\,(\cos\theta) \tag{10}$$

where θ = angle between the ray and the light vector. The attenuation due to the density function along a ray can be calculated as:

$$\exp\left(-\tau\int_{t_1}^{t_2} D(s)\, ds\right) \tag{11}$$

where τ = proportionality constant between density and attenuation. The intensity of the light that arrives to the view point along the direction of R due to all the elements along the ray is given by:

$$B = \int_{t_1}^{t_2} \left(\exp\left(-\tau\int_{t_1}^{t} D(s)ds\right) \right) \left(I(t)D(t)P(\cos\theta) \right) dt \tag{12}$$

The attenuation is represented in the view plane (2D image) using a correspondent colour. Thus each a pixel in the image plane has an associated colour according to the interaction of the ray with the volume.

Figure 8 shows a 3D image of the LV based on this method. The apparent no uniformity of the volume is a consequence of the free-hand technique.
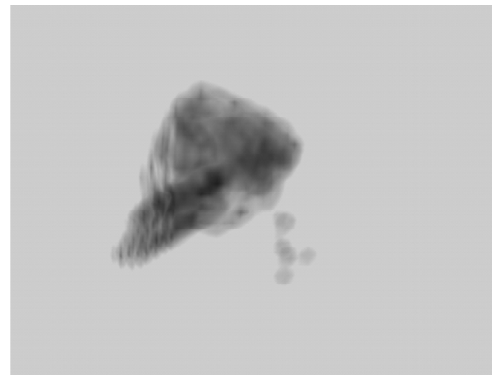
Figure 8: Volume Visualisation of the LV

6.2. Isosurface

Isosurfaces show 3-D scalar fields by drawing surfaces that represent points of constant values. The isosurfaces representation uses the Marching Cubes algorithm [William&Cline 1987] (implemented using vtkMarchingCubes) that is a divide-and-conquer approach to locate the surface in a logical cube created

from eight pixels. The values of the eight corners of the cube are used to determine how the surface intersects this cube. To find the surface intersection in the cube, it is assigned a value '1' to the cube's vertex if the data value at that vertex exceeds (or equals) the value of the surface to be constructed. These vertices are considered inside the surface. Cube vertices with values below the surface value receive a 'zero' and are considered outside the surface. The surface intersects those cube edges where one vertex is outside the surface and the other is inside the surface. With this assumption, the topology of the surface within the cube is determined. In 3D space there are 256 different situations for the marching cubes representation but using rotations and symmetries they can be generalized in 15 families. Figure 9 shows an isosurface visualisation for the left ventricle. Using exactly the same images and the same defined isosurface level, the segmentation method developed was compared with a manual one, where the contour points were defined by the user. The image on the left is based on the automatic segmentation explained before and the right one is the result of a manual segmentation.
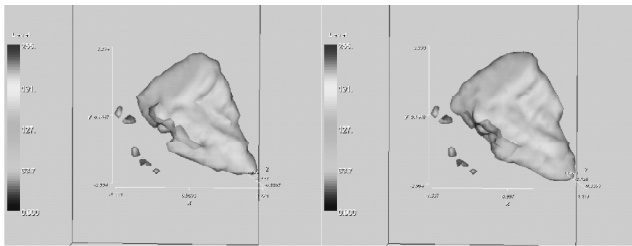
Figure 9: **Isosurface Visualisation using Gaussian Interpolation with Automatic (left) and Manual (right) Segmentation**

This application offers the possibility for the user to modify the isosurface level using the simple cursor. The visualized data is automatically updated and the operator can also obtain the volume value of the rendered object. The calculation of this value (implemented using vtkMassProperties) is based on the discrete form of the divergence theorem [Alyassin 1994].

6.3. Slicing

Slicing allows the user to select different volume perspectives of the organ being studied. This is a visualisation technique that performs cuts through the data. In particular the slicing operation was implemented with a plane as a cutting function. Data attributes are then mapped onto the cut surface [Shroeder & al 2004]. In practice this application allows us to perform cuts in the 3D volume. The user can automatically see the cuts in the three principal axes (x, y, and z) and it also provides the option of cutting an arbitrary plane. This arbitrary plane is selected using the cursor to change the plane orientation. This is important when particular region of the volume need to be analysed. All combinations of the

four different cuts are permitted. These cuts are 2D images that have associated to each pixel a colour representation of the voxel intensity that is cut by the plane. Figure 10 illustrates cuts along the three major axes and also along an arbitrary plane.

6.3.1. Picking Attributes

In a clinical environment it becomes necessary to determine some surface attributes such as a distance between two points in a particular plane cut or between two different cuts. This functionality becomes important to determine dimensional characteristics of live organs that from the simple B-scan images would not be possible. For the analysis referenced in this paper, this tool can be used for the quantitative measurement of LV volumes from 2D images by the modified Simpson´s rule, for instance, in which the calculation of volume involves the summation of the areas of the 20 elliptical discs from their diameters [Setarehdan & Soraghan 1998].

This application provides the user with the ability to measure every desired parameter (implemented with vtkMath) and view the point coordinates (implemented with vtkCellPicker) using simply the left and right mouse buttons. For every interaction picking important points, the measured value is automatically updated. Figure 11 illustrates the picking point's functionality.
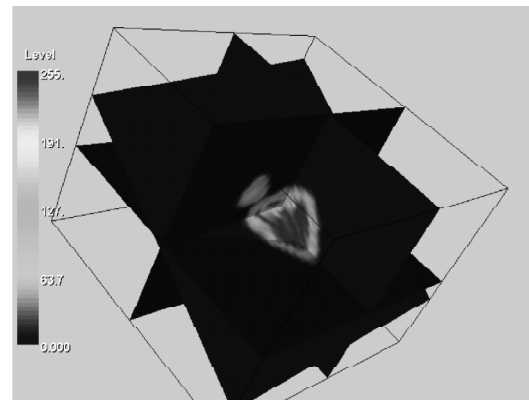
Figure 10: Visualisation of the Three Plane Cuts: Along the three Major Axes (x, y, z) and an Arbitrary Plane
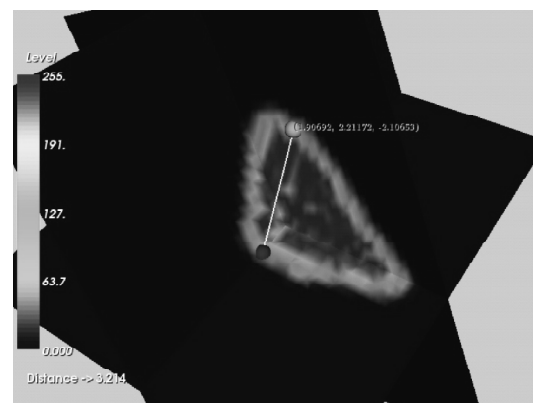
Figure 11: Point Selection for Coordinates Measurement

7. CONCLUSIONS

The developed medical interface for echographic images presents as an important and valuable tool for a variety of clinical applications. Technicians are able to acquire and select the most important B-scan images in real-time, manipulate them and make 3D reconstruction in an acceptable time. Almost everything related with the volumetric reconstruction of freehand 2D images can be done with this tool. This tool is dynamic being in continuous expansion for additional functions. Some of the most important ones are the possibility to perform a registration process, the automatic left ventricle central point determination (which is crucial for the developed segmentation process), a 4D visualisation and obtaining some important cardiac parameters like stroke volume and ejection fraction.

Another important step is the application of the segmentation process to the entire cardiac cycle. In this presentation the acquired images were selected accordingly with a specific time in the cardiac cycle (accomplished with the help of the ECG). All considered images represent the ventricle in the systole stage. As future work, and aiming the continuous development of the tool, it is our intention to provide to the user the capability to visualise the left ventricle model during the entire cardiac cycle, showing the movement from systole to diastole.

It was demonstrated that the most difficult task associated with this application is the images segmentation. The used technique, combining the radial and parallel search-based edge detection, has proved to be effective in the boundaries extraction even for the noisy and low quality images analysed. The results of the developed segmentation process were approved by the physicians that performed most of the image acquisition using the system described earlier. It is important to mention that the tested algorithm was applied to noisy and low resolution images, and we demonstrated that images presenting better qualities give rise to extracted contours significantly improved.

As already referred, this application tool was developed with the help of technicians who have given valuable and important suggestions in its construction. According to them, the image processing time is acceptable if the central point determination could be automatic. Additional improvements must be considered respecting to image selection along with the cardiac cycle. This also leads to a considerable reduction of the processing time.

REFERENCES

[1] Alyassin A. M. & al. (1994), Evaluation of New Algorithms for the Interactive Measurement of Surface Area and Volume, *Med Phys* 21(6).

[2] Chu C. H. & al. (1988), Detecting Left-ventricular Endocardial and Epicardial Boundaries by Digital Two-dimensional Echocardiography, 7: 81-90.

[3] Detmer, P. R. & al. (1990), Matched Filter Identification of Left-ventricular Endocardial Borders in Transesophageal Echocardiograms. *IEEE Trans. Med. Imag.*, 9: 396-404.

[4] Frangi, A. & al. (2001), Three-dimensional Modeling for Functional Analysis of Cardiac Images: A Review. *IEEE Transactions on Medical Imaging* 20(1): 2–25.

[5] Hoppe, H. (1994), PhD Thesis, Dept. of Computer Science and Engineering, University of Washington, June. *IEEE Trans. Med. Imag.*, 7: 81-90.

[6] Melton, H. E. & al. (1983), Automatic Real-time Endocardial Edge Detection in Two-dimensional Echocardiography. *Ultrason. Imag.*, 5: 300-307.

[7] More, J. (1977), "The Levenberg Marquardt Algorithm: Implementation and Theory", Springer-Verlag.

[8] Otsu, N. (1979), "A Threshold Selection Method from Gray Level Histogram," *IEEE Trans. Systems, Man., and Cybernetics*, vol. SMC-8, pp. 62-66.

[9] Setarehdan, S. K. & Soraghan, J. J. (1998), "Cardiac Left Ventricular Volume Changes Assessment by Long Axis Echocardiographical Image Processing", *IEE Proceedings-Vision, Image and Signal Processing*, 145(3): 203-212.

[10] Shroeder, W. & al. (2004), The Visualization Toolkit An Object-Oriented Approach To 3D Graphics Kitware, Inc (3th Edition).

[11] Varandas, J. & al. (2004), VOLUS–A Visualization System for 3D Ultrasound Data. *Ultrasonics* 42: 689–694.

[12] Xujiong, Y. & Noble, J. A. (2002), 3-D Freehand Echocardiography for Automatic Left Ventricle Reconstruction and Analysis Based on Multiple Acoustic Windows, *IEEE Trans. On Medical Imaging*, 21(9): 1051-58.

[13] Watt A. & Watt M. (1992), Advanced Animation and Rendering Techniques: Theory and Practice, Addison-Wesley, Reading, Massachusetts.